CONSIDERATION OF LASER PULSE FLUCTUATIONS AND AUTOMATIC GAIN CONTROL IN RADIOMETRIC CALIBRATION OF AIRBORNE LASER SCANNING DATA

Hubert Lehner[a], Helmut Kager[a], Andreas Roncat[a] and András Zlinszky[b]

[a]Institute of Photogrammetry and Remote Sensing,
Vienna University of Technology, Gusshausstrasse 27-19, 1040 Vienna, Austria,
(hl, hk, ar)@ipf.tuwien.ac.at
[b]Balaton Limnological Research Institute of the Hungarian Academy of Sciences,
Klebelsberg Kuno t 3, 8237 Tihany, Hungary
azlinszky@tres.blki.hu

Commission VI/5

KEY WORDS: Airborne Laser Scanning, Full Waveform, Radiometric Calibration, Emitted Pulse Energy Fluctuations, Automatic Gain Control

ABSTRACT:

ALS has become a standard tool for high-resolution topographic mapping within the last two decades. Besides the geometric data in form of three-dimensional point clouds, also radiometric information is available in form of amplitude and width of the backscattered echo (the latter is provided by full waveform (FWF) systems only). However, these radiometric observables need to be calibrated. Influences originate not only from the factors included in the radar equation, but also from fluctuations of the emitted laser pulse and from automatic gain control (AGC) devices. These two influences are investigated in detail in this study on behalf of the two data sets acquired with a FWF capable Riegl LMS-Q560 system and a Leica ALS50-II discrete echo system. It could be shown that the influences of laser pulse fluctuations and AGC can be removed to a certain extent. This way, radiometric calibration can be performed more reliably.

1 INTRODUCTION

Airborne laser scanning (ALS) is well known for its capability to accurately and densely sample the terrain surface and is thus widely used for topographic mapping. Besides the 3D coordinates of the sampled surface points also the signal strength of the returns, which carries information about the surface's backscattering characteristics, is measured. While discrete ALS systems directly store this signal strength in form of an amplitude measurement (often referred to as intensity), full waveform (FWF) ALS systems enable the extraction of the amplitude and additionally also the echo width from the recorded waveform in the post processing. Only recently these physical observables of the signal strengths have become of greater interest and thus are more and more investigated in order to use them as additional information channel for analysing surface characteristics.

However, these signal strength measurements are affected by several factors, such as range, angle of incidence and atmospheric attenuation. Absolute radiometric calibration (Lehner and Briese, 2010) proved to be able to transfer the physical observables into absolute radiometric values free from these influencing factors (see section 2.1). This study investigates two additional factors: (1) fluctuation of the emitted laser pulses and (2) automatic gain control (AGC), which amplifies the received signal strength in order to keep it within the range of the receiver (see sections 2.2 and 2.3 respectively). The variations of the emitted pulse are a transmitter property and were studied on a full waveform data set acquired with a Riegl LMS-Q560. The AGC, on the other hand, is a receiver property and was investigated on a discrete echo data set originating from a Leica ALS50-II system. The data sets and the derived results are presented in section 3. Conslusions are given in section 4.

2 THEORY

2.1 Radiometric Calibration

The LIDAR adapted formulation of the radar equation (see equation (1)) relates the product of system waveform amplitude and width, $\hat{S}s_s$, to the product of echo amplitude and width, $\hat{P}_i s_{p,i}$. The first is directly proportional to the emitted laser power while the latter is directly proportional to the detected power. Furthermore, the following influencing factors are considered: the diameter of the receiver aperture D_r, the range between sensor and target R, the backscattering coefficient of the surface γ as well as transmission factors for the system and the atmosphere η_{sys} and η_{atm} (Wagner, 2010):

$$\hat{P}_i s_{p,i} = \frac{\hat{S}s_s D_r^2}{16 R_i^2} \cdot \eta_{sys}\eta_{atm} \cdot \gamma_i \tag{1}$$

The backscattering coefficient γ is normalised to the laser's transverse area and thus independent of R and the beam divergence of the ALS system. With respect to typical ALS wavelengths most surfaces can be assumed to be diffuse (Lambertian) reflecting. For such surfaces the backscattering coefficient γ_d depends simply on the reflectance ρ_d of the surface and the angle of incidence θ (Lehner, 2011):

$$\gamma_{d,i} = 4 \cdot \rho_{d,i} \cdot \cos\theta_i \tag{2}$$

Unkown parameters in equation (1) are D_r and η_{sys}, which are assumed to be constant for one specific ALS system. Using meteorological observation data, η_{atm} can be accounted for (Höfle and Pfeifer, 2007, Lehner, 2011). The correction for atmospheric

transmission is important in case of multi temporal analysis. During one flight campaign, however, η_{atm} can be assumed to be rather constant. Therefore, it was neglected in this study. Finally, the emitted laser pulse parameters $\hat{S}s_s$ are typically unknown, which is why they are treated as constant as well (see section 2.2). Combining all these parameters in the calibration constant C_{cal} (see right equation of (3)) yields the basic calibration equation (left equation of (3)):

$$\tilde{\rho}_{d,i} = \frac{C_{cal} R_i^2 \hat{P}_i s_{p,i}}{4 \cos\theta_i} \quad \text{with} \quad C_{cal} = \frac{16}{D_r^2 \hat{S}s_s \eta_{sys} \eta_{atm}} \tag{3}$$

Based on these equations, an absolute calibration procedure and software (opalsRadioCal module (IPF, 2010)) were developed. Details concerning the method and the workflow can be found in (Briese et al., 2008) and (Lehner and Briese, 2010) and (Lehner, 2011). The method is based on in-situ reflectance measurement of a reference surface. (Briese et al., 2008) and (Lehner, 2011) use a Riegl reflectometer and Spectralon® diffuse reflectance standards (Labsphere Inc., 2010) for the estimation of the reflectance of the calibration targets (in the following indicated by the subscript CT) but any other measurement system providing this information can be used as well. However, it is crucial that the measurement device measures at the same wavelength as the ALS system, since the reflectance of a specific surface can vary a lot between different wavelengths. Based on the ALS echoes hitting the calibration targets, a mean calibration constant can be estimated by the following equation:

$$C_{cal} = \frac{1}{N_{CT}} \sum_{j=1}^{N_{CT}} \frac{4\, \tilde{\rho}_{CT,j}\, \cos\theta_j}{R_j^2\, \hat{P}_j\, s_{p,j}} \tag{4}$$

This calibration constant can be used consecutively to calibrate the whole data set.

2.2 Laser Pulse Fluctuations

As can be seen in equation (1), the strength of the emitted laser pulse affects the return power. ALS manufacturers, however, try to keep this factor at different levels as constant as possible, wherefore most correction and calibration methods treat it as constant. Higher flight heights require higher levels of pulse energy in order to guarantee that the reflected signal is still strong enough to be recorded. To reach higher pulse energies, the laser needs more time for pumping, which, in turn, results in lower pulse repetition rates. (Chasmer et al., 2005) report e.g. pulse energies in dependence on selectable pulse repetition frequencies (PRF) for different discrete echo ALS systems of Optech. This means that according to the flight height a suitable pair of PRF and pulse energy level has to be chosen when planning the flight campaign. Furthermore, the chosen energy level can be considered within radiometric correction (Höfle and Pfeifer, 2007, Ahokas et al., 2006).

Besides these general changes of emitted pulse energy within different levels, also fluctuations within one specific level might occur. FWF ALS systems, e.g. the Riegl LMS-Q560, do not only record the temporal shape of the received echoes but also the shape of a damped copy of the emitted pulse (Roncat et al., 2011). This information per pulse enables to study the fluctuations in emitted pulse energy. Moreover, it enables to consider the emitted pulse energy during the radiometric calibration process per laser shot by simply moving the shot-based system waveform parameters $\hat{\mathbf{S}}_\mathbf{i}\mathbf{s}_{\mathbf{s},\mathbf{i}}$ (see equations (3)) from the right equation to the left equation:

$$\tilde{\rho}_{d,i} = \frac{C_{cal} R^2 \hat{P}_i s_{p,i}}{4 \cos\theta_i\, \hat{\mathbf{S}}_\mathbf{i}\mathbf{s}_{\mathbf{s},\mathbf{i}}} \quad \text{with} \quad C_{cal} = \frac{16}{D_r^2 \eta_{sys} \eta_{atm}} \tag{5}$$

This, however, requires the system waveform amplitude $\hat{\mathbf{S}}_\mathbf{i}$ and width $\mathbf{s}_{\mathbf{s},\mathbf{i}}$ as additional attributes per echo, which leads to higher storage space and processing time. Alternatively, echo parameters normalized by the parameters of the individual laser pulses can be used instead of the original echo amplitudes and echo widths (see (Roncat et al., 2011)). For analysis and visualization purposes the first approach was chosen for this study and equations (5) were used to perform the radiometric calibration.

2.3 Automatic Gain Control

Some ALS systems, e.g. the discrete echo ALS system Leica ALS50-II, use an adjustable automatic gain control (AGC) device, which amplifies the received echo amplitudes in order to keep it within an 8 bit range. The value of the AGC is measured and recorded as an 8 bit value per pulse as well. The general idea of such a device is that if the returning signal strength is too low, the AGC increases to the next higher level and thus also the recorded amplitude value increases. Accordingly, the AGC decreases in case the signal strengths are too high in order to decrease the amplitude measurements. The information on the technical background of AGC is sparse. However, some more information including a correction approach can be found in (Vain et al., 2010).

Based on the information we have, we know that the recorded amplitude (intensity) $\hat{P}_{i,g}$, the gain function G of the recorded gain value g and the received signal amplitude $\hat{P}_i$ are presumably related to each other as follows:

$$\hat{P}_i = \frac{\hat{P}_{i,g}}{G(g)} \tag{6}$$

The studied data originates from the discrete echo ALS system Leica ALS50-II (see section 3.1), which is why no echo widths are available. Therefore, they are treated as constant and $\mathbf{s}_{\mathbf{p},\mathbf{i}}$ is moved from the left to the right equation as $\mathbf{s}_\mathbf{p}$. Possible echo widening is, thus, ignored. Furthermore, the Leica ALS50-II does not record the system waveform. Thus, equations (3) take the following form:

$$\tilde{\rho}_{d,i} = \frac{C_{cal} R_i^2\, \hat{\mathbf{P}}_{\mathbf{i},\mathbf{g}}}{4 \cos\theta_i\, \mathbf{G}(\mathbf{g})} \quad \text{with} \quad C_{cal} = \frac{16\, \mathbf{s_p}}{D_r^2 \hat{S}s_s \eta_{sys} \eta_{atm}} \tag{7}$$

Accordingly, equation (4) results to:

$$C_{cal} = \frac{1}{N_{CT}} \sum_{j=1}^{N_{CT}} \frac{4\, \tilde{\rho}_{CT,j}\, \cos\theta_j\, \mathbf{G}(\mathbf{g})}{R_j^2 \qquad \hat{\mathbf{P}}_{\mathbf{j},\mathbf{g}}} \tag{8}$$

Regarding a specific gain value g the gain function $G(g)$ is constant and can, thus, be factored out of the sum $\sum$. Calculating the sum for every g individually results in the g-dependent calibration

constants $\tilde{C}_{cal,g}$, which can be related to the overall calibration constant by the gain function:

$$C_{cal} = G(g)\,\tilde{C}_{cal,g} = G(g)\,\frac{1}{N_{CT}}\sum_{j=1}^{N_{CT}}\frac{4\,\tilde{\rho}_{CT,j}\,\cos\theta_j}{R_j^2\quad\hat{P}_{j,g}} \qquad (9)$$

Based on equation (9) two specific gain functions were investigated and their parameters α and β were determined by least squares adjustment (see section 3). The $\tilde{C}_{cal,g}$ values (see figure 8, which is derived from the data presented in figure 7) served as observations for the least squares adjustment and their reciprocal variances as weights, whereas C_{cal}, α and β are the unknowns to be estimated.

$$G_1(g) = e^{\alpha g+\beta} = e^{\alpha g}\cdot e^{\beta} \qquad (10)$$

Since $e^{\alpha g+\beta}$ can be reformulated as $e^{\alpha g}\cdot e^{\beta}$, the term β results in a factor which just increases or decreases the calibration constant. Therefore, it cancels out when applied in equation (7). As a second function a linear approach was tested:

$$G_2(g) = \alpha g + \beta = \lambda\,(\bar{\alpha} g + \bar{\beta}) \qquad (11)$$

Here a similar situation occurs: λ is considered as a common factor of α and β and thus also of C_{cal}. In order to perform least squares adjustment out of the three parameters a suitable one has to be chosen ($\neq 0$) so that the others can be derived.

3 RESULTS AND DISCUSSION

3.1 Data Sets

The effect of the laser pulse fluctuations on radiometric calibration was tested on one flight strip of the Vienna wide ALS campaign carried out at the end of 2006 and beginning of 2007. The data of this flight strip was acquired on December 27$^{\text{th}}$ 2006, by the company Diamond Airborne Sensing GmbH with a Riegl LMS-Q560, which operates at a wavelength of 1550 nm. The scan frequency was 200 kHz, the aircraft speed above ground 150 km/h, the flying height above ground 500 m and the scan angle $\pm$ 30°. These settings resulted in a swath overlap of about 60 %, a mean point density of more than 20 measurements per square meter and a laser footprint size on the ground of about 25 cm.

The strip data covers parts of Schönbrunn palace and garden. The particular test site chosen for this study was the parade yard of Maria Theresia casern (see figure 1) in the south of Schönbrunn area since it features a very large area with homogeneous scattering properties. Its reflectance was measured with the Riegl reflectometer and Spectralon reflectance standards to 23.5 $\pm$ 1.8 % (Lehner and Briese, 2010).

While all nine asphalted tiles (highlighted in figure 1 by blue and red squares) were used in order to calculate the calibration constant, only one tile (highlighted in figure 1 by the red square) was used to analyse the effect of laser pulse variations on the calibrated diffuse reflectance measure values (see next section).

The effect of AGC was investigated on ALS data collected during the EUFAR AIMWETLAB survey in August of 2010, using

Figure 1: RGB-Orthophoto of Maria Theresia casern in the south of Schönbrunn gardens (MA41, 2010). The reference areas (parade yard asphalt) are highlighted in blue and out of those the studied tile is highlighted in red.

a Leica ALS50-II sensor operated from the Dornier Do 228 of the NERC Airborne Research and Survey Facility. This sensor operates in the 1064 nm wavelength, and scans with an oscillating mirror, creating a sinusoidal pattern of points on the ground. The surveyed area was the shore zone of Lake Balaton and the area of the Kis-Balaton wetland. The detailed rationale and full technical background of the survey is explained in (Zlinszky et al., 2011). Out of this data set two flight strips were used in this study, which were acquired utilizing the following settings: The scan frequency was 45 kHz, the aircraft speed above ground 250 km/h, the flying height above ground 1500 m and the scan angle about $\pm$ 20°. These settings resulted in a swath overlap of about 30 %, a mean point density of 1 measurement per square meter and a laser footprint size on the ground of about 20 cm.

A bare soil and a white gravel area served as calibration targets (see figure 2(a)). Their reflectances were determined by an ASD FieldSpec 3 spectrometer and a Spectralon reflectance standard to 13.8 $\pm$ 2.0 % for the bare soil and 53.5 $\pm$ 3.8 % for the white gravel. Additionally, a parking space (white gravel as well) and a sports field (see figure 2(b)) were used for the analysis. While only one flight strip covers the reference surfaces, the additional study areas are covered by both flight strips.

3.2 Laser Pulse Fluctuations

As presented in section 3.1, only one asphalted square of the parade yard of Maria Theresia casern was used for the analysis of the laser pulse fluctuations on radiometric calibration. The selected echoes are presented in figure 3, grey-coded according to their corresponding laser pulse amplitudes. Flight direction was approximately from north to south. It can clearly be seen that the laser pulse amplitudes vary considerably. However, the variations within one scan line seem to be lower than between different scan lines resulting in two significantly dark bands in scan direction.

Figure 4 presents the calibrated diffuse reflectance measure values of the test area plotted against their corresponding emitted pulse amplitude: (a) when neglecting the laser pulse variations (see equation (3)) and (b) when considering those variations (see equation (5)). Additionally, linear regression lines are plotted in order to better visualise the trends.

As can be expected, when neglecting the shot-based laser pulse parameters, the diffuse reflectance measure values of echoes originating from lower pulse energies are lower and the ones from higher pulse energies are higher. After considering the laser pulse parameters in the calibration process, an approximately but not totally horizontal line can be seen for the linear regression. This means that the data fits the physical model presented in section 2.2 much better and compensating for fluctuations in emitted pulse energy in this way is appropriate.

(a)

(b)

Figure 2: RGB-Aerial images covered by one flight strip of the Balaton flight campaign: (a) bare soil and white gravel served as reference surfaces (highlighted in blue) and (b) additionally studied surfaces highlighted in red, namely a parking site covered with white gravel and an asphalted sports field.

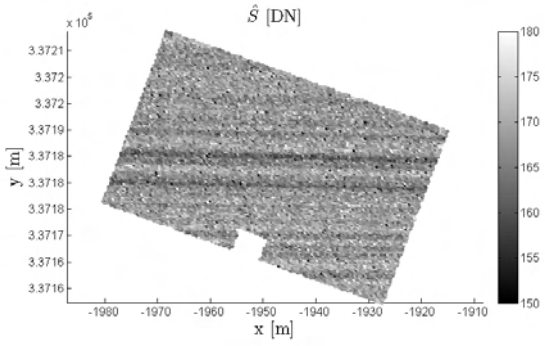

Figure 3: Points within the studied asphalt area (see figure 1) grey-coded according to their individual emitted laser pulse amplitudes.

3.3 Automatic Gain Control

Compensating for gain changes due to the automatic gain control faces the problem that the gain function is unknown and has to be determined before the calibration constant can be derived. This first step was achieved using the two reference surfaces (see section 3.1). Figure 5 presents the echoes of the bare soil target: (a) grey-coded according to their corresponding gain value and (b) the recorded amplitudes accordingly. In figure 5(a), it can be seen that consecutive scan lines are characterised by alternating higher and lower gain value. Thus, this effect can also be seen in figure 5(b).

Figure 6 presents the recorded echoes and the gain values of all test areas and for both flight strips as histograms. The histograms of the sports field have a very characteristic shape, meaning they consist of two bumps. The same would be the case for the high reflecting parking space. However, the second bump is recorded under oversaturation of the receiver with the value 255 for most

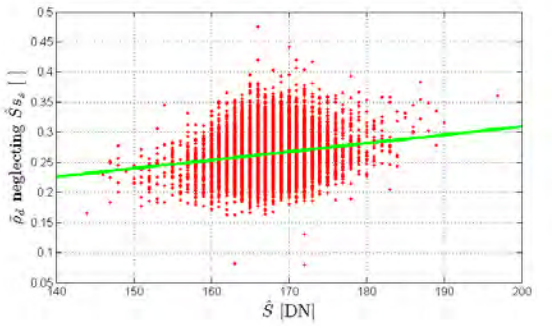

(a)

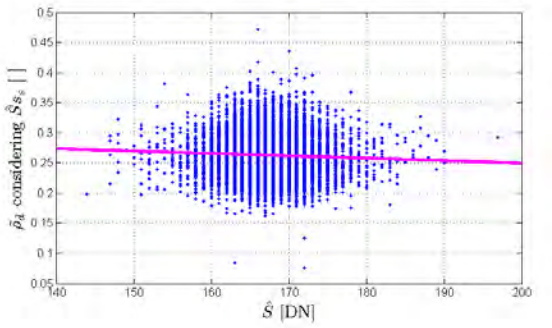

(b)

Figure 4: Diffuse reflectance measure $\tilde{\rho}_d$ when neglecting (a) and considering (b) the laser pulse variations. The green and magenta line represent the linear regression lines.

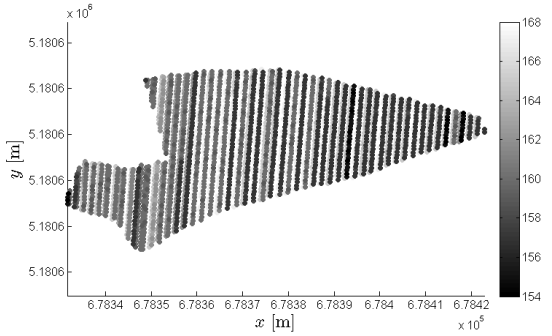

(a) AGC values g

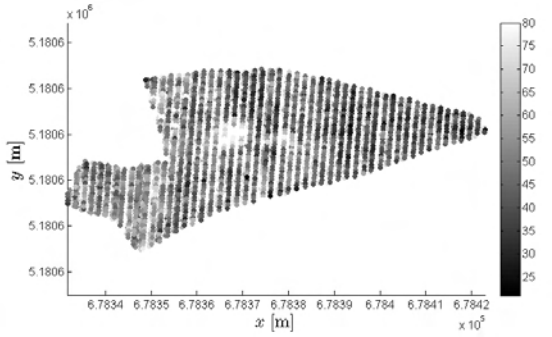

(b) recorded amplitude values $\hat{P}_{j,g}$

Figure 5: Points within the bare soil area (see figure 2(a)) grey-coded according to their corresponding gain value (a) and according to their recorded amplitude (b).

echoes. Thus, these echoes were excluded from further processing. For the reference areas the gain values do not just jump from

one extreme to the other, which is why only one bump can be observed there.

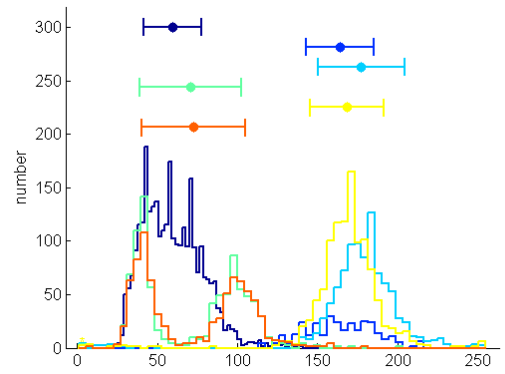

(a) recorded amplitude values $\hat{P}_{j,g}$

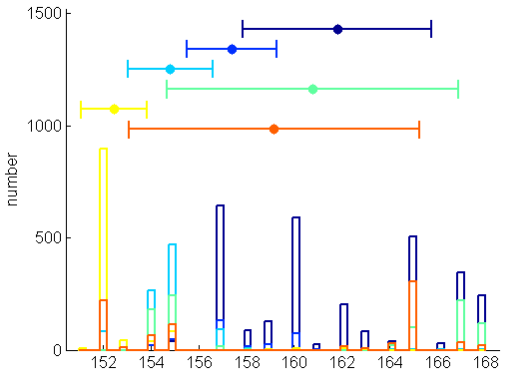

(b) AGC values g

Figure 6: Histograms of the recorded amplitude (a) and gain values (b) with their error bars from top till down: bare soil (dark blue), white gravel (blue), parking space (light blue), sports field (green) and finally parking space (yellow) and sports field (orange) for the second flight strip.

Figure 7 presents the echo amplitudes plotted against their corresponding gain value for the bare soil (a) and the white gravel area (b). As was expected, with increasing gain value the echo amplitudes increase as well. The error bars of the data points are additionally plotted on top of them.

As mentioned in section 2.3, the gain function was unknown (i.e. not revealed by the manufacturer). Thus, an exponential and a linear gain function were investigated. In order to perform least squares adjustment based on equation (9), the $\tilde{C}_{cal,g}$ values were calculated. These mean values and corresponding error bars for both reference surfaces are presented in figure 8. At first sight it can be seen that the $\tilde{C}_{cal,g}$ values for the lower and higher reflecting reference surface match quite well.

Based on these $\tilde{C}_{cal,g}$ observations (mean and variance), the parameters α and β for both gain functions were determined using least squares adjustment. Afterwards, the gain functions were used to derive a global calibration constant in order to perform radiometric calibration of the whole data set. Figure 9 presents histograms of the resulting diffuse reflectance measure values separately for each test area and for both flight strips as in figure 6. As quality criteria of the gain function it is assumed that the bumps of the test areas, which are recorded in both flight strips, coincide. This is, however, not the case for both gain functions. Using the

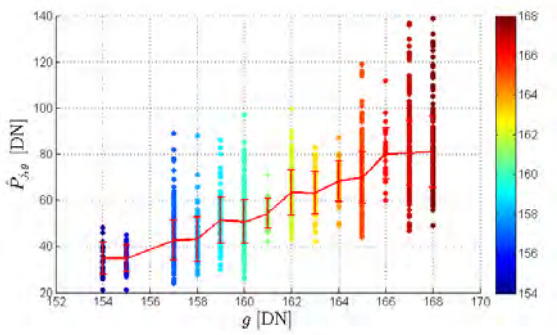

(a) bare soil reference area

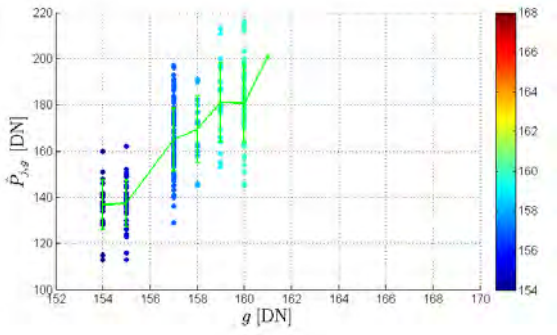

(b) white gravel reference area

Figure 7: Recorded echo amplitudes of the echoes within the bare soil reference surface (a) and within the white gravel surface (b) plotted against their corresponding gain value. The line represents the mean value of $\hat{P}_{j,g}$ for a certain g and the error bars their standard deviation.

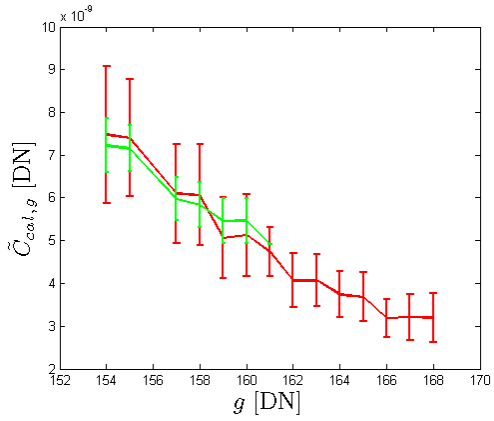

Figure 8: $\tilde{C}_{cal,g}$ (mean values with error bars) derived for the two reference surfaces.

linear gain function, the peaks of the bumps of the parking space echoes are clearly separable from each other (see figure 9(b)). The corresponding peaks utilizing the exponential function are much closer to each other, though. Thus, it can be concluded that the exponential function characterises the gain function better than the linear function.

As mentioned in section 3.1, the reflectances for the test areas are 13.8 % and 53.5 %. The gain values for the echoes within the reference areas were in the range of 154 to 168. Thus, for higher reflecting surfaces as well as for gain values outside the specific gain range of the reference surfaces, the gain functions with the determined coefficients extrapolate. Reference surfaces with higher reflectance and surfaces which are acquired at other

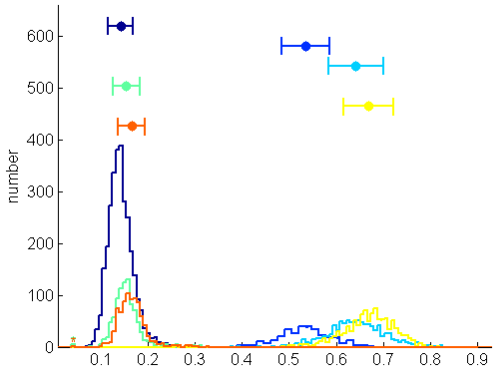

(a) $\tilde{\rho}_d$ utilizing the exponential gain function $G_1(g)$

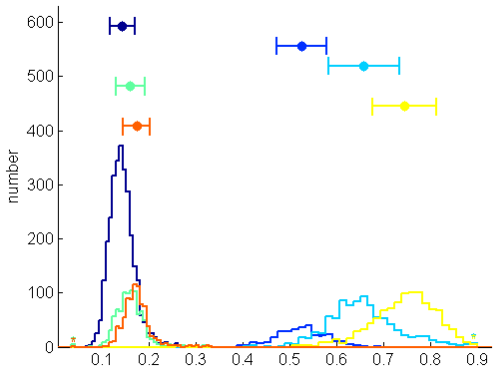

(b) $\tilde{\rho}_d$ utilizing the linear gain function $G_2(g)$

Figure 9: Histograms of the diffuse reflectance measure $\tilde{\rho}_d$ calculated using the exponential gain function $G_1(g)$ (see equation (10)) (a), and the linear gain function $G_2(g)$ (see equation (11)) (b) with their error bars from top till down: bare soil, white gravel, parking space, sports field and then parking space and sports field for the second flight strip.

gain values would be necessary for a better estimation of the gain function coefficients.

4 CONCLUSION

In order to increase radiometric accuracy, influencing factors such as emitted laser pulse energies or gain values have to be considered in case they are available. Calibrated reflectance values are supposed to enhance point based classification, which is a valuable input for further applications.

ACKNOWLEDGEMENTS

We would like to thank Stadtvermessung Wien, Magistratsabteilung 41 (MA41, 2010), for providing the full-waveform ALS data, which was used for this study. Furthermore, we would like to thank the company Riegl Laser Measurement Systems GmbH (RIEGL, 2010) for providing the reflectometer.

The Lake Balaton ALS survey has received fundings from the European Community's 7th Framework Programme (FP7/2008-20012) under EUFAR contract n 2271. The research activities of A. Zlinszky at the IPF were supported by the Ernst-Mach Scholarship of the Stiftung Aktion Österreich-Ungarn.

REFERENCES

Ahokas, E., Kaasalainen, S., Hyyppä, J. and Suomalainen, J., 2006. Calibration of the Optech ALTM 3100 laser scanner intensity data using brightness targets. International Archives of the Photogrammetry, Remote Sensing and Spatial Information Sciences XXXVI, Part A1, pp. CD–ROM, T03–11.

Briese, C., Höfle, B., Lehner, H., Wagner, W., Pfennigbauer, M. and Ullrich, A., 2008. Calibration of full-waveform airborne laser scanning data for object classification. In: M. D. Turner and G. W. Kamerman (eds), Laser Radar Technology and Applications XIII, Proceedings of SPIE, Vol. 6950, SPIE Press, pp. 69500H–69500H–8.

Chasmer, L., Hopkinson, C., Smith, B. and Treitz, P., 2005. Examining the influence of laser pulse repetition frequencies on conifer forest canopy returns. Oral presentation at the conference Silviscan - LIDAR applications in forest assessment and inventory, September 29-October 1, 2005, Blacksburg, Virginia, USA.

Höfle, B. and Pfeifer, N., 2007. Correction of laser scanning intensity data: data and model-driven approaches and applications. ISPRS Journal of Photogrammetry and Remote Sensing 62(6), pp. 415–433.

IPF, 2010. Institute of Photogrammetry and Remote Sensing (IPF) of the Vienna University of Technology, OPALS - Orientation and Processing of Airborne Laser Scanning data. `http://www.ipf.tuwien.ac.at/opals/opals_docu/index.html`. visited on 03/06/2010.

Labsphere Inc., 2010. Spectralon - Diffuse Reflectance Standards. `http://www.labsphere.com/data/userFiles/DiffuseReflectanceStandardsProductSheet_7.pdf`. visited on 03/06/2010.

Lehner, H., 2011. Radiometric calibration of airborne laser scanner data. Master's thesis, Institut für Photogrammetrie und Fernerkundung der Technischen Universität Wien.

Lehner, H. and Briese, C., 2010. Radiometric calibration of full-waveform airborne laser scanning data based on natural surfaces. International Archives of Photogrammetry, Remote Sensing and Spatial Information Sciences XXXVIII, Part 7B, pp. 360–365.

MA41, 2010. Stadtvermessung Wien, Magistratsabteilung 41. `http://www.wien.gv.at/stadtentwicklung/stadtvermessung/index.html`. visited on 03/06/2010.

RIEGL, 2010. Riegl Laser Measurement Systems GmbH. `http://www.riegl.com/`. visited on 03/06/2010.

Roncat, A., Lehner, H. and Briese, C., 2011. Laser pulse variations and their influence on radiometric calibration of full-waveform laser scanner data. ISPRS Workshop "Laser Scanning 2011". To appear.

Vain, A., Yu, X., Kaasalainen, S. and Hyyppä, J., 2010. Correcting airborne laser scanning intensity data for automatic gain control effect. IEEE Geoscience and Remote Sensing Letters 7(3), pp. 511–514.

Wagner, W., 2010. Radiometric calibration of small-footprint full-waveform airborne laser scanner measurements: Basic physical concepts. ISPRS Journal of Photogrammetry and Remote Sensing 65(6), pp. 505–513.

Zlinszky, A., Tóth, V., Pomogyi, P. and Timár, G., 2011. Initial report of the AIMWETLAB project: simultaneous airborne hyperspectral, LIDAR and photogrammetric survey of the full shoreline of Lake Balaton, Hungary. Geographia Technica 1, pp. 101–117.